NATIONAL ADVISORY COMMITTEE FOR AERONAUTICS

TECHNICAL NOTE 2111

A STUDY OF WATER PRESSURE DISTRIBUTIONS DURING LANDINGS WITH SPECIAL REFERENCE TO A PRISMATIC MODEL HAVING A HEAVY BEAM LOADING AND A 30° ANGLE OF DEAD RISE

By Robert F. Smiley

Langley Aeronautical Laboratory
Langley Air Force Base, Va.

Washington
July 1950

NATIONAL ADVISORY COMMITTEE FOR AERONAUTICS

TECHNICAL NOTE 2111

A STUDY OF WATER PRESSURE DISTRIBUTIONS DURING LANDINGS WITH SPECIAL REFERENCE TO A PRISMATIC MODEL HAVING A HEAVY BEAM LOADING AND A 30° ANGLE OF DEAD RISE

By Robert F. Smiley

SUMMARY

A landing investigation is being conducted at the Langley impact basin to obtain some quantitative measurements of the distribution of water pressure during landings, which may serve as an aid in the establishment of seaplane design criteria and in determining the value of the existing hydrodynamic pressure theories. This paper presents pressure measurements obtained on a 5-foot prismatic model having an angle of dead rise of 30°, a beam of 1 foot, and a beam-loading coefficient of 18.8. This model was subjected to smooth-water landings at fixed trims of 6°, 15°, 30°, and 45° for a range of flight-path angles from approximately 2° to 20°.

Initial impact conditions and maximum pressures are presented for all landings together with time histories of the velocities and pressure distributions for several representative landings. The instantaneous pressures for a given draft, trim, and location on the hull bottom are found to be directly proportional to the square of the velocity normal to the keel.

Comparisons of the experimental pressures and theoretical pressures indicate the degree of correlation and some limitations of the available theoretical treatments.

INTRODUCTION

Inasmuch as the magnitude and distribution of the hydrodynamic loads imposed on seaplane hulls during landings is a matter of concern to seaplane designers, an appreciable amount of research has been conducted to obtain reliable means of predicting these loads. In recent years much of this research has been concerned with the over-all loads problem, for some phases of which theories have been developed and subsequently substantiated by experimental investigations. In general,

however, a knowledge of the over-all loads is not a sufficient criterion for local structural design since, during seaplane landings, large and irregular pressure gradients usually exist over the hull bottom such that the local pressures greatly exceed the average pressures.

Much of the available information relevant to the problem of determining these local pressures is contained in references 1 to 11. References 1 to 4 deal with theoretical aspects of the problem, references 1 to 3 being concerned primarily with the pressures on transverse sections of a prismatic hull where the chines do not penetrate the fluid surface and reference 4 being concerned with the pressures at transverse sections where the chines are immersed in the fluid. Some experimental data obtained under controlled conditions are given in references 3, 6, 7, and 8. Data are also available from several full-scale landing tests. Although all these data and theory comprise a definite contribution to the solution of the problem of hydrodynamic load distribution, large gaps remain to be filled by accurate experimental investigation and by further theoretical studies.

As a step to provide more extensive hydrodynamic pressure-distribution data a landing investigation is being conducted at the Langley impact basin on a series of prismatic hull and float models of varying dead rise and beam loading. Tests have been completed on a model having a beam-loading coefficient of 18.8, a beam of 1 foot, and a 5-foot prismatic section having an angle of dead rise of 30°. Fixed-trim landings were made in smooth water for a large range of trims, velocities, and flight-path angles; and during each landing time histories of the pressures, velocities, and over-all loads were recorded.

This paper presents the experimental pressure-distribution and velocity data obtained from these tests. The data are analyzed to show the effects of velocity, flight-path angle, trim, draft, and location on the hull bottom. Comparisons are made between these experimental pressures and theoretical pressures from references 1 to 4 in order to establish the value and limitations of the various theories.

SYMBOLS

b	beam of model, feet
c	wetted semiwidth at any station along keel, feet
$\dot{r}$	equivalent planing velocity, feet per second $\left(\frac{\dot{z}}{\sin \tau}\right)$
g	acceleration due to gravity, 32.2 feet per second per second

h	theoretical constant $\left(\frac{\pi - 2\beta_r}{\pi}\right)$
k	theoretical constant defined in appendix B
m	mass of model, slugs
p	instantaneous pressure, pounds per square inch
s	longitudinal distance from step to any point on hull bottom, feet
$\dot{s}$	instantaneous velocity of model parallel to keel, feet per second ($\dot{x} \cos \tau - \dot{y} \sin \tau$)
t	time after water contact, seconds
u	theoretical constant $\left(\frac{2}{\pi} \tan \beta\right)$
V	instantaneous resultant velocity of model, feet per second
V_w	wave velocity, feet per second
V_{wi}	wind velocity, feet per second
x	transverse distance from keel to any point on hull bottom, feet
$\dot{x}$	instantaneous velocity of model parallel to undisturbed water surface, feet per second
y	instantaneous draft of model normal to undisturbed water surface, feet
$\dot{y}$	instantaneous velocity of model normal to undisturbed water surface, feet per second
$\dot{z}$	instantaneous velocity of model normal to keel, feet per second ($\dot{x} \sin \tau + \dot{y} \cos \tau$)
$\ddot{z}$	instantaneous acceleration of model normal to keel, feet per second per second
β	angle of dead rise, degrees
β_e	effective angle of dead rise, degrees

γ instantaneous flight-path angle, degrees

λ auxiliary variable used for integration and as a parameter in appendix B, radians

μ theoretical constant $\left(\frac{2}{\pi}\tan\beta_e\right)$

ρ mass density of water, 1.938 slugs per cubic foot

τ trim, degrees

τ_w angle of wave slope

Subscripts:

a two-dimensional flow

o at water contact

p peak value

r radian measure

Dimensionless variables:

C_Δ beam-loading coefficient $\left(\frac{m}{\rho b^3}\right)$

$\frac{p}{\frac{1}{2}\rho\dot{z}^2}$ pressure coefficient based on $\dot{z}$

$\frac{p}{\frac{1}{2}\rho\dot{f}^2}$ pressure coefficient based on $\dot{f}$

$\frac{p}{\frac{1}{2}\rho V^2}$ pressure coefficient based on V

APPARATUS

The investigation was conducted in the Langley impact basin with the test equipment and instrumentation described in reference 9. The

test model was 1 foot wide and had a dead-rise angle of 30° and a prismatic section for a length of 5 feet. The lines and pertinent dimensions of the model are shown in figure 1 and a photograph of the model is shown as figure 2.

The instrumentation used to measure horizontal velocity and vertical velocity is described in reference 9. Accelerations in the vertical direction were measured by a standard NACA air-damped accelerometer having a natural frequency of 16.5 cycles per second with approximately 0.65 critical damping and a range from -1g to 6g. Pitching moments were obtained from an electrical strain-gage-type dynamometer. The times of water contact and exit of the model were determined by means of an electrical circuit completed by the water. Pressures were measured with 20 gages distributed over the hull bottom as shown in figure 1. These gages had flat $\frac{1}{2}$-inch-diameter diaphragms which were mounted flush with the hull bottom. Motion of a metal rod attached to the center of the diaphragm unbalanced an inductive electrical bridge circuit inside the gage. The resulting current, proportional to the pressure on the diaphragm, was amplified by 5000-cycle carrier amplifiers and recorded on a 24 channel oscillograph. Natural frequencies of the gages were approximately 3300 cycles per second and the response of the recording system was faithful to at least several hundred cycles per second. A typical oscillograph record is shown in figure 3.

PRECISION

The instrumentation used in these tests gives measurements that are believed accurate within the following limits:

Horizontal velocity, feet per second	±0.5
Vertical velocity at water contact, feet per second	±0.2
Weight, pounds	±2
Vertical acceleration, percent	±5
Pitching moment about step, percent	±8
Pressure, pounds per square inch	[a]±2 ±0.1p
Time, seconds	±0.005

[a]There are some indications of larger errors due to frequency response for runs 6 and 7.

TEST PROCEDURE

The model was tested at 0° yaw and at fixed trims of 6°, 15°, 30°, and 45° in smooth water. A series of landings was made with the model

loaded to a weight of 1172 pounds, which corresponded to a beam-loading coefficient of 18.8. The flight-path angle was varied over a range from approximately 3° to 20° for the tests with 30° and 45° trim, from 2° to 6° for the 15° trim, and was limited to 2° for the 6° trim. Most of the landings were repeated under as similar conditions as possible in order to check the consistency of the experimental measurements.

During each landing a compressed-air engine (described in reference 9) exerted a vertical lift force on the model equal to its weight so that the model entered the water with constant vertical velocity; otherwise the model was free to move in the vertical direction. The model was attached to a towing carriage weighing approximately 5600 pounds. Because of this large added carriage inertia the model did not slow down significantly (horizontally) during any landing.

RESULTS

The basic data obtained from the present investigation are presented in tables I and II and in figure 4. The initial vertical velocities, horizontal velocities, and trims for all runs are presented in table I together with the values of the maximum pressures recorded on each pressure gage. In table II are tabulated the instantaneous vertical velocities corresponding to the peak pressures for several of the pressure gages. The corresponding instantaneous horizontal velocities are substantially the values given in table I since the change in horizontal velocity during any impact was small. In figure 4 extensive time-history pressure distributions are given for one run at each trim together with several less extensive distributions from other runs. (The boundary of the wetted surface as indicated in this figure was arbitrarily drawn as a straight line slightly forward of the line of maximum pressure. These lines are believed to give a reasonable estimate of the wetted area, but they do not necessarily give an accurate representation of the wave rise.)

In order to provide an independent check on the accuracy of these pressure data the following procedure was used: For several runs, pressure distributions were read at the time of maximum load on the model. These distributions were integrated to obtain the maximum vertical load and the pitching moment about the step at the time of maximum load. In figure 5 the results of these integrations are compared with the corresponding values obtained from the accelerometer and load-measuring dynamometer. (The dynamometer measured the pitching moment about an axis remote from the step. In order to transfer this moment to the step the accelerometer reading was used.) The close agreement of these independent measurements appears to substantiate the over-all reliability of these pressure measurements. It is realized that this check does not

preclude the possibility that the pressure gages did not respond faithfully to the localized high-frequency pressure transients which occurred near the peak pressures during some of these landings since such localized effects would have had little influence on the over-all integrated pressure distributions. Analysis of the data (to be discussed subsequently) indicates, however, that in general the peak values are also reliable.

DISCUSSION

Independence of Pressure Coefficient $\frac{p}{\frac{1}{2}\rho\dot{z}^2}$ and Flight-Path Angle

Pressure-distribution data from figure 4 are plotted in figures 6 to 9 as the variation of the dimensionless pressure coefficient $\frac{p}{\frac{1}{2}\rho\dot{z}^2}$ for various immersions and trims. Data for different landing conditions and for the same immersion and trim have been superimposed in the same three-dimensional plots.

From theoretical considerations discussed in appendix A it would be expected that these pressure coefficients would be essentially independent of the instantaneous flight-path angle or, for a given trim, draft, and location on the hull bottom, the pressures should be directly proportional to the square of the velocity normal to the keel. That such is the case can be seen by an examination of figures 7 to 9. For the 15° trim data in figure 7(c) the pressure coefficient appears fairly constant for flight-path angles of 0.6° and 5.7°. An apparent reduction in peak pressure occurs for runs 6 and 7; however, these two runs had the highest vertical velocities of the 15° trim runs and the pressure transients in the vicinity of the peak pressures may possibly have occurred too rapidly to permit the recording system to follow them accurately. The additional 15° trim data in figure 7(d) show much better agreement between the pressure coefficients at flight-path angles of −2.4° and 4.5°. For the trim of 30°, the pressure coefficients for different flight-path angles are closely similar, for angles of 2.3°, 9.0°, and 19.2° in figure 8(b) and for angles of 7.1° and 18.2° in figure 8(c). Similarly, at 45° trim the agreement is good for flight-path angles of 1.5°, 8.9°, and 18.1° in figure 9(b) and for angles of −4.4°, 6.3°, and 16.1° in figure 9(c). In summary, the experimental pressure coefficients obtained during this investigation appear to be relatively independent of the instantaneous flight-path angle. (This observed general independence of the pressure coefficients and the flight-path angle serves to indicate that most of the experimental data, including the peak values, are free from frequency-response errors inasmuch as any such effects would, in general, produce an apparent variation of pressure coefficient with flight-path angle.)

Distribution of Pressure Coefficient $\frac{p}{\frac{1}{2}\rho\dot{z}^2}$

The forces on non-chine-immersed transverse sections of a prismatic float (fig. 10) are generally considered to be relatively independent of the wetted length. Consequently, this model at any given trim would be expected to have a characteristic (of the trim) pressure distribution on the triangular projected area, the transverse sections of which have no chine immersion. Prior to chine immersion this characteristic pressure distribution should be reduced near the step to conform to the condition of approximately atmospheric pressure at the step. Subsequent to chine immersion, when a rectangular pressure area is present aft of the triangular area (fig. 10), less step effect exists and the pressures on the triangular projected area should be somewhat larger than was the case prior to chine immersion. Aft of the triangular area, in sections where the chines are immersed, the pressures should decrease so that they approach zero near the step. As the wetted length increases the longitudinal pressure gradients should then become smaller. The experimental data in figures 6 to 9 show all these expected trends. In addition at the 6° trim (fig. 6) small localized negative pressures occur near the step.

Variation of Pressure Coefficient $\frac{p}{\frac{1}{2}\rho\dot{z}^2}$ with Trim

Transverse sections without chine immersion.- At very small trims of a few degrees or less the flow about non-chine-immersed sections of a fixed-trim prismatic hull (fig. 10) may be considered to occur in two-dimensional planes stationary in space and oriented normal to the keel (references 10 and 11). Then for very small trims the pressure coefficient $\frac{p}{\frac{1}{2}\rho\dot{z}^2}$ (acceleration effects being neglected) should be the same at each transverse section and should be independent of the trim. Wagner (references 1 and 2) has given approximate equations for the pressure distribution for this limiting case (see appendix B). The theoretical pressure distribution for a dead-rise angle of 30° was calculated from these equations and is shown with the experimental data both in figures 6 and 7. (Because of the large differences in magnitude between the experimental and theoretical pressures at the 30° and 45° trims, this theoretical distribution has been omitted in figs. 8 and 9.) Fair agreement is seen to exist with the theory at the 6° trim except in the vicinity of the step. At the other trims (15°, 30°, and 45°) the agreement is poor, the theoretical pressures being much larger than the experimental pressures. Thus, the simple assumption of the Wagner-type flow in two-dimensional planes normal to the keel is indicated not to be satisfactory for the range of trim of the present investigation.

It is evident from figures 6 to 9 that the experimental pressure coefficients do decrease with increase of trim. At the low trims (6° and 15°) there are large peaks at the edge of the wetted area. At the higher trims (15° and 30°) the coefficients tend to become higher at the keel and lower toward the chines. Some consideration of this effect has been made by Pierson (reference 3). He has determined an effective dead-rise angle which depends on the trim and dead-rise angle (appendix B). Wagner's equations are used with this effective dead rise rather than with the actual dead rise in order to calculate the pressure coefficient at a finite trim. Pressure coefficients calculated with the use of this modification of Pierson's are shown in figures 6 to 8. It is seen that, except in the vicinity of the step, good agreement exists with the experimental data at the trims of 6° and 15°. The theoretical pressures are too small at 30° trim and no comparison is possible at 45°. (Since the effective dead rise given by Pierson in reference 3 is only an approximation which was used there for a 6° trim, it was hardly expected to be valid for the extreme trims of this investigation. Also it is evident that the approximation is invalid at trims above 33° for this dead rise since $\sin \beta_e > 1$.)

Transverse sections with chine immersion.- Figures 6 to 9 show that at all trims the transverse pressure distributions on chine-immersed sections (fig. 10) are approximately elliptical and are smaller than or equal to the pressures on the sections without chine immersion. At the 6° trim the longitudinal pressure gradients along the chine-immersed length of the float are generally small. At the 15° trim large longitudinal pressure gradients occur. Above 15° trim for a given wetted length the longitudinal gradients decrease with increased trim.

As a theoretical approach to the pressures on chine-immersed sections Korvin-Kroukovsky and Chabrow (reference 4) have presented a derivation for the pressure on a two-dimensional wedge with chines immersed in a fluid with separated flow behind the wedge. As a first approximation the resulting equations are applied to the three-dimensional case by considering the flow to occur primarily in two-dimensional planes normal to the keel (appendix B). With the use of this modification, theoretical pressure distributions were calculated and are shown in figures 6 to 9 together with the experimental data. The theoretical pressure coefficients $\frac{p}{\frac{1}{2}\rho \dot{z}^2}$ predicted in this way are always less than one and are the same at each transverse section; whereas an examination of figures 6 to 9 shows that the experimental data for chine-immersed sections of the hull show in general much larger coefficients and longitudinal pressure gradients. At 6° trim the pressure is approximately four times the predicted value. As the trim or wetted length increases the pressure coefficients decrease until at the largest trim (45°) and longest wetted length fair agreement exists between the theoretical and experimental pressures.

Effect of Deceleration

In the preceding discussion and in the theoretical pressure distributions plotted in figures 6 to 9 no consideration was made of the effect of the deceleration of the model on the pressure distribution. If the model is decelerating in the direction normal to the keel (as in these tests), negative increments of pressure will exist which as a first approximation are proportional to the deceleration of the model and are distributed elliptically over the wetted width (appendix B). The maximum theoretical negative increment of pressure according to this first approximation is $\rho\ddot{z}c$, which quantity (for the conditions of these tests) was always less than 1 pound per square inch which is of the same order of magnitude as the experimental error. Consequently, rather than to complicate greatly the comparison of experimental and theoretical distributions by the consideration of this term it was considered better to omit the term.

Peak Pressures

The peak pressure coefficients obtained during this investigation were the largest near the keel. Outboard from the keel the peak pressure coefficients were slightly smaller and near the step they were considerably smaller (figs. 6 to 9). The slightly higher pressures at the keel may be partly attributed to a $\frac{1}{4}$-inch radius rounding of the keel, but that this rounding would have had any substantial effect is unlikely.

At low angles of trim the peak pressure coefficient $\frac{p_p}{\frac{1}{2}\rho\dot{z}^2}$ should be independent of trim and wetted area. According to Wagner this value for small angles of dead rise $(\beta \to 0)$ is (appendix B)

$$\frac{p_p}{\frac{1}{2}\rho\dot{z}^2} = \left(\frac{\pi}{2} \cot \beta\right)^2 \tag{1}$$

At very high trims the peak pressure coefficient $\frac{p_p}{\frac{1}{2}\rho\dot{z}^2}$ should become smaller and approach the value (appendix A)

$$\frac{p_p}{\frac{1}{2}\rho\dot{z}^2} = \frac{1}{\sin^2\tau} \tag{2}$$

or the peak pressure coefficient $\frac{p_p}{\frac{1}{2}\rho\dot{f}^2}$ should approach 1. The peak pressures for the three gages which had the highest pressures throughout these tests are plotted in figure 11 against $\frac{1}{2}\rho\dot{z}^2$. These particular gages (numbered as 5, 6, and 7 in fig. 1) were located near the keel at positions removed from the step. The faired straight lines drawn through the data were used to obtain peak pressure coefficients for each trim. These peak pressure coefficients are plotted in figure 12 against trim as a percentage of the limiting value at 90°, that is, as the coefficient $\frac{p_p}{\frac{1}{2}\rho\dot{f}^2}$. The experimental data are seen to agree fairly well with Wagner's theory and with Pierson's modification for trims below 15°. At higher trims neither theory is adequate and the data rapidly approach the upper limiting value of 1. An empirical formula

$$\frac{p_p}{\frac{1}{2}\rho\dot{f}^2} = \frac{\pi^2\tan^2\tau}{\pi^2\tan^2\tau + 4\tan^2\beta} \tag{3}$$

is shown which does fit the two endpoints given by equations (1) and (2) ($\tau \longrightarrow 0^\circ$ and $\tau \longrightarrow 90^\circ$) and which is in fair agreement with the experimental data over the entire range of trim.

Whereas an analysis of the data in terms of the peak pressure coefficient $\frac{p_p}{\frac{1}{2}\rho\dot{z}^2}$ or $\frac{p_p}{\frac{1}{2}\rho\dot{f}^2}$ was most expedient, for practical purposes, the use of a pressure coefficient based on the resultant velocity is desirable. Equation (3), so converted, becomes

$$\frac{p_p}{\frac{1}{2}\rho V^2} = \frac{\pi^2\sin^2(\gamma + \tau)}{\pi^2\sin^2\tau + 4\tan^2\beta\cos^2\tau} \tag{3a}$$

This coefficient is shown in figure 13 as the variation of the peak pressure coefficient with trim for various flight-path angles. The maximum coefficient at each trim is also shown.

CONCLUSIONS

From an analysis of the experimental data obtained during a smooth-water landing investigation of a prismatic float having a high beam-loading coefficient, the following conclusions may be drawn:

1. For a given trim, draft, and location on the hull bottom the instantaneous pressures are directly proportional to the square of the velocity normal to the keel but are independent of the instantaneous flight-path angle.

2. In the region forward of the immersed chines

   a. At the low trims (6° and 15°) large pressure peaks exist at the edge of the wetted area. At the higher trims (30° and 45°) the distributions tend to become higher at the keel and lower toward the chines.

   b. The ratio of pressure to the square of the normal velocity decreases with increased trim.

   c. Wagner's theory gives a pressure distribution which is in fair agreement with the 6° trim data except in the vicinity of the step. At the other trims (15°, 30°, and 45°) the agreement is poor, the theoretical pressures being much larger than the experimental pressures.

   d. Pierson's modification of Wagner's theory gives a pressure distribution which, except in the vicinity of the step, is in good agreement with the experimental data for the 6° and 15° trims. The theoretical pressures are too small at the 30° trim.

3. In the region where the chines are immersed

   a. The longitudinal pressure gradient is small at the 6° trim, large at the 15° trim, and decreases with further increases of trim.

   b. Use of the two-dimensional analysis of Korvin-Kroukovsky and Chabrow gives theoretical pressures which are in general smaller than the experimental pressures, but at the largest trim (45°) and longest wetted length fair agreement exists.

4. Wagner's and Pierson's equations give a fair estimate of the largest peak pressures for trims below 15°, but are inadequate for the higher trims.

5. The largest peak pressures can be represented with fair accuracy over the entire range of trim by the empirical equation

$$\frac{p_p}{\frac{1}{2}\rho V^2} = \frac{\pi^2 \sin^2(\gamma + \tau)}{\pi^2 \sin^2\tau + 4 \tan^2\beta \cos^2\tau}$$

where p_p is the peak pressure, ρ is the mass density, V is the resultant velocity, τ is the trim, β is the angle of dead rise, and γ is the flight-path angle.

Langley Aeronautical Laboratory
National Advisory Committee for Aeronautics
Langley Air Force Base, Va., February 17, 1950

APPENDIX A

REMARKS ON THEORETICAL BACKGROUND

Landing Impact

In the impact of long narrow prismatic floats (fig. 10) the instantaneous pressures can be considered as a first approximation to be composed of two terms: one proportional to the square of the instantaneous velocity of the model normal to the keel, and one proportional to the acceleration normal to the keel (references 10 and 11). For the special case of a model having a wing lift equal to the model weight and when no other external forces are present (as was the case for the model of this paper) the sum of the two force terms (proportional to $\dot{z}^2$ and $\ddot{z}$) is proportional to the normal acceleration of the model (from Newton's second law) from which fact it is evident that the normal acceleration is proportional to the square of the normal velocity. The factor of proportionality varies with the impact geometry (shape of model, trim, and draft) and the beam-loading coefficient. Then for this special case the dimensionless pressure coefficient based on the normal velocity $\frac{p}{\frac{1}{2}\rho\dot{z}^2}$, for a given location on the hull bottom, should depend only on the impact geometry and the beam-loading coefficient. Also, if the ratio of the acceleration force to the velocity-squared force be small (which may often be the case for heavy beam loadings) then, regardless of the wing lift and beam loading, the pressure coefficient $\frac{p}{\frac{1}{2}\rho\dot{z}^2}$ should depend essentially only on the impact geometry and should be independent of the beam loading.

Relation to Steady Planing

The preceding discussion indicates that for a long narrow prismatic model the steady planing condition differs from the corresponding impact condition (same draft, trim, shape of model, and normal velocity) only by the effect of normal acceleration. The impact-velocity component corresponding to the steady planing velocity (which is $\frac{\dot{z}}{\sin\tau}$ in terms of the normal velocity) is $\frac{\dot{z}}{\sin\tau} = \dot{x} + \dot{y}\cot\tau = \dot{f}$. Then since in steady planing all pressures are less than or equal to the dynamic pressure corresponding to the resultant planing velocity (buoyancy being neglected) and the peak pressure approaches this value at high trims, the same should be true during impact for the velocity $\dot{f}$.

In general, the acceleration on a float during impact is negative or opposite to the direction of normal motion (as was the case throughout these tests) such that negative increments of pressure are created on the hull bottom. Then, in general, the impact-pressure coefficients $\frac{p}{\frac{1}{2}\rho\dot{z}^2}$ should be somewhat less than the corresponding planing coefficients.

APPENDIX B

EQUATIONS FOR THEORETICAL PRESSURE DISTRIBUTIONS

Wagner (reference 1) has presented a derivation for the pressure distribution on a two-dimensional symmetric body of small slope dropping on a smooth fluid surface. The resulting equation is

$$\frac{p}{\rho} = \frac{V_a^2}{u} \frac{1}{\sqrt{1 - \left(\frac{x}{c}\right)^2}} + \frac{dV_a}{dt} \sqrt{c^2 - x^2} - \frac{1}{2} \frac{V_a^2}{\left(\frac{c}{x}\right)^2 - 1} \tag{B1}$$

where c is the wetted semiwidth of the body, x is the width corresponding to any point on the body, V_a is the two-dimensional velocity of the body, and u is $\frac{2}{\pi} \tan \beta$ for a V-bottom surface. For the case of a three-dimensional prismatic float at an angle of trim, Wagner (reference 2) gives the velocity corresponding to V_a as

$$V_a = V\gamma_r + (V - V_{wi})\tau_r + V_w\tau_{w_r} \tag{B2}$$

where V_{wi} is the wind velocity, V_w is the wave velocity, and τ_{w_r} is the wave slope. In the absence of wind and waves this is

$$V_a = V(\gamma_r + \tau_r) \tag{B3}$$

Since Wagner considered small angles, equation (B3) is essentially

$$V_a = V \sin(\gamma + \tau) = \dot{z} \tag{B4}$$

(Equation (B4) is seen to be equivalent to the statement that the flow about a prismatic float at an angle of trim occurs primarily in two-dimensional planes stationary in space and oriented normal to the keel.) Combining equations (B1) and (B4) with $u = \frac{2}{\pi} \tan \beta$ gives a first approximation for the transverse pressure distribution on a V-bottom float at sections having no chine immersion

$$p = \frac{1}{2}\rho\dot{z}^2\left(\frac{\pi \cot \beta}{\sqrt{1 - \left(\frac{x}{c}\right)^2}} - \frac{1}{\left(\frac{c}{x}\right)^2 - 1}\right) + \rho\ddot{z}\sqrt{c^2 - x^2} \tag{B5}$$

where the first two terms are seen to give the pressure for constant velocity and the last term is proportional to the normal deceleration of the float. Pierson (reference 3) has modified Wagner's equations to include better the effects of trim. For the case of steady planing he gives the equation

$$p = \frac{\rho \dot{z}^2}{\mu}\left(\frac{1}{\sqrt{1 - \left(\frac{x}{c}\right)^2}} - \frac{\frac{\mu}{2}}{\left(\frac{c}{x}\right)^2 - 1}\right) \tag{B6}$$

where $\mu = \frac{2}{\pi} \tan \beta_e$ and β_e, called the effective angle of dead rise, is defined by the relation $\sin^2\beta_e = \sin^2\beta + \frac{\pi^2}{4} \sin^2\tau$. Then,

$$p = \frac{1}{2}\rho \dot{z}^2\left(\frac{\pi \cot \beta_e}{\sqrt{1 - \left(\frac{x}{c}\right)^2}} - \frac{1}{\left(\frac{c}{x}\right)^2 - 1}\right) \tag{B7}$$

The peak pressures on the float are given by Wagner (reference 2) for small angles of dead rise $(\beta \to 0)$ as

$$p_p = \frac{1}{2}\rho\left(\frac{dc}{dt}\right)^2 \tag{B8}$$

where

$$\frac{dc}{dt} = \frac{V_a}{u}$$

Combining equations (B4) and (B8) with $u = \frac{2}{\pi} \tan \beta$ gives

$$p_p = \frac{1}{2}\rho \dot{z}^2\left(\frac{\pi^2}{4} \cot^2\beta\right) \tag{B9}$$

Modified peak pressures may be obtained from the maximum value of equation (B7).

Korvin-Kroukovsky and Chabrow (reference 4) have presented a derivation for the pressure distribution on a symmetric two-dimensional wedge completely submerged in a fluid, moving normal to the stream, and having steady separated flow behind the wedge. The resulting pressure equation is

$$p = \frac{1}{2}\rho V_a^2 \left[1 - \left(\frac{\cos \lambda}{1 + \sin \lambda}\right)^{2h}\right] \tag{B10}$$

where λ is defined by the relations

$$x = 2kb \cos \beta \int_{\lambda}^{\frac{\pi}{2}} (1 + \sin \lambda)^h (\cos \lambda)^{1-h} \sin \lambda \, d\lambda$$

$$\frac{1}{k} = 4 \cos \beta \int_{0}^{\frac{\pi}{2}} (1 + \sin \lambda)^h (\cos \lambda)^{1-h} \sin \lambda \, d\lambda$$

and

$$h = \frac{\pi - 2\beta_r}{\pi}$$

By combining equations (B4) and (B10) a first approximation is obtained for the pressures on chine-immersed sections of a V-bottom hull

$$p = \frac{1}{2}\rho \dot{z}^2 \left[1 - \left(\frac{\cos \lambda}{1 + \sin \lambda}\right)^{2h}\right] \tag{B11}$$

REFERENCES

1. Wagner, Herbert: Über Stoss- und Gleitvorgänge an der Oberfläche von Flussigkeiten. Z.f.a.M.M., Bd. 12, Heft 4, Aug. 1932, pp. 193–215.

2. Wagner, Herbert: Landing of Seaplanes. NACA TM 622, 1931.

3. Pierson, John D.: On the Pressure Distribution for a Wedge Penetrating a Fluid Surface. Rep. No. 336, Stevens Inst. Tech., June 1948.

4. Korvin-Kroukovsky, B. V., and Chabrow, Faye R.: The Discontinuous Fluid Flow Past an Immersed Wedge. Rep. No. 334, Stevens Inst. Tech., Oct. 1948.

5. Lamb, Horace: Hydrodynamics. Sixth ed., Cambridge Univ. Press, 1932, pp. 94–105.

6. Jones, E. T., and Blundell, R. W.: Force and Pressure Measurements on V-Shapes on Impact with Water Compared with Theory and Seaplane Alighting Results. R. & M. No. 1932, British A.R.C., 1938.

7. Jones, E. T.: Some Measurements of Pressure over a Vee-Shape When Dropped into Water. R. & M. No. 2312, British A.R.C., 1935.

8. Sottorf, W.: Experiments with Planing Surfaces. NACA TM 739, 1934.

9. Batterson, Sidney A.: The NACA Impact Basin and Water Landing Tests of a Float Model at Various Velocities and Weights. NACA Rep. 795, 1944.

10. Mayo, Wilbur L.: Analysis and Modification of Theory for Impact of Seaplanes on Water. NACA Rep. 810, 1945.

11. Milwitzky, Benjamin: A Generalized Theoretical and Experimental Investigation of the Motions and Hydrodynamic Loads Experienced by V-Bottom Seaplanes during Step-Landing Impacts. NACA TN 1516, 1948.

TABLE I

INITIAL IMPACT CONDITIONS AND MAXIMUM BOTTOM PRESSURES

Pressure-gage positions				1	2	3	4	5	6	7	8	9	10	11	12	13	14	15	16	17	18	19	20	21
Run	τ (deg)	$\dot{y}_o$ (fps)	$\dot{x}_o$ (fps)	Pressure (lb/sq in.)																				
1	6	2.9	90.9	4.8	2.9	5.7	2.4	6.7	5.5	----	5.2	6.3	0	5.7	0	0	0	0	0	0	0	--	3.7	2.7
2		3.0	89.3	5.4	2.8	5.8	2.7	8.1	6.5	5.0	6.8	6.0	0	6.1	6.8	0	0	0	0	0	0	--	4.8	2.8
3	15	3.4	89.3	18.3	14.4	15.8	10.7	27.8	24.1	0	0	0	0	0	0	0	0	0	0	0	0	--	13.4	0
4		3.4	89.3	19.1	14.1	16.2	11.7	27.5	24.3	0	0	0	0	0	0	0	0	0	0	0	0	--	16.2	0
5		5.7	90.9	20.2	16.5	17.8	13.3	28.9	29.9	24.3	16.5	0	0	0	0	0	0	0	0	0	0	--	16.7	0
6		9.3	90.1	22.3	19.8	19.9	15.3	31.3	31.0	32.9	30.2	27.6	20.7	----	28.2	0	0	0	0	0	0	--	19.3	24.7
7		9.4	90.9	26.2	22.2	22.7	17.7	----	33.5	31.1	33.0	29.4	23.6	33.8	----	0	0	0	0	0	0	--	21.0	25.6
8	30	5.1	92.0	35.3	28.8	26.7	21.2	----	----	0	0	0	0	0	0	0	0	0	0	0	0	--	26.6	0
9		7.4	90.9	43.0	31.5	29.2	23.4	53.8	45.5	0	0	0	0	0	0	0	0	0	0	0	0	--	29.2	0
10		7.5	90.9	43.5	32.6	25.3	22.0	44.7	50.8	0	0	0	0	0	0	0	0	0	0	0	0	--	30.6	0
11		7.5	90.9	46.0	34.9	30.8	23.4	48.5	52.8	0	0	0	0	0	0	0	0	0	0	0	0	--	32.1	0
12		7.5	90.9	46.0	32.6	30.5	8.8	47.4	52.3	0	0	0	0	0	0	0	0	0	0	0	0	--	26.0	0
13		7.6	90.9	48.9	34.7	31.0	14.2	46.0	52.5	0	0	0	0	0	0	0	0	0	0	0	0	--	29.5	0
14		7.7	90.9	44.4	36.5	32.8	25.6	46.1	53.5	0	0	0	0	0	0	0	0	0	0	0	0	--	31.8	0
15		9.3	51.6	18.7	14.0	14.6	11.8	23.5	22.5	20.0	17.4	15.1	9.4	21.5	0	0	0	0	0	0	0	--	14.6	13.0
16		9.4	50.0	16.2	12.7	13.7	10.1	20.4	20.5	19.2	14.3	14.3	8.7	19.1	0	0	0	0	0	0	0	--	12.5	10.7
17		9.3	25.0	6.5	5.4	5.7	4.9	8.7	8.5	7.5	7.0	6.0	3.7	10.5	6.5	6.3	5.1	4.4	3.7	5.3	0	--	5.5	5.4
18	45	5.9	89.3	46.2	37.1	36.2	27.5	----	0	0	0	0	0	0	0	0	0	0	0	0	0	--	35.7	0
19		8.3	90.9	49.6	38.2	----	29.5	59.0	47.0	0	0	0	0	0	0	0	0	0	0	0	0	--	38.6	0
20		8.3	90.9	53.3	38.4	35.5	18.5	60.0	46.3	0	0	0	0	0	0	0	0	0	0	0	0	--	36.6	0
21		9.5	50.5	18.4	13.8	15.5	12.7	20.7	19.9	16.6	13.9	13.0	7.7	1.3	0	0	0	0	0	0	0	--	14.2	10.4
22		9.6	50.5	18.1	14.9	15.6	10.9	21.0	19.8	----	12.9	13.7	7.1	----	0	0	0	0	0	0	0	--	14.8	9.7
23		9.4	27.8	7.5	6.3	6.9	5.0	8.0	8.0	7.1	6.4	5.6	3.2	7.7	5.4	4.2	3.3	2.4	1.5	0	0	--	6.4	4.2
24		9.6	27.2	6.9	5.0	6.2	4.5	8.6	7.6	6.8	4.5	5.6	2.6	5.5	3.5	3.4	2.1	2.4	.6	0	0	--	5.6	3.5

TABLE II

PEAK PRESSURES AND CORRESPONDING INSTANTANEOUS VERTICAL VELOCITIES

Run	Trim (deg)	Gage 5				Gage 6				Gage 7			
		1st peak		2d peak		1st peak		2d peak		1st peak		2d peak	
		p (psi)	$\dot{y}$ (fps)	p (psi)	$\dot{y}$ (fps)	p (psi)	$\dot{y}$ (fps)	p (psi)	$\dot{y}$ (fps)	p (psi)	$\dot{y}$ (fps)	p (psi)	$\dot{y}$ (fps)
1	6	6.7	2.9	4.2	−1.8	5.5	2.8	3.0	−1.7	----	----	----	----
2		8.1	3.0	4.2	−1.7	6.5	2.8	3.1	−1.7	5.0	2.6	3.2	−1.4
3	15	27.8	3.2	18.9	−2.4	24.1	1.0	22.4	−0.1	(a)	(a)	(a)	(a)
4		27.5	3.1	20.0	−2.3	24.3	1.0	22.2	0	(a)	(a)	(a)	(a)
5		28.9	5.6	16.6	−3.7	29.9	4.9	19.4	−3.0	24.3	3.0	16.2	−1.3
6		31.2	9.2	14.2	−5.4	31.0	8.8	14.4	−4.9	32.9	8.0	15.0	−4.4
7		----	----	11.2	−5.6	33.5	9.0	13.8	−5.0	31.1	7.9	16.1	−4.6
8	30	----	----	36.0	−2.9	----	----	----	----	(a)	(a)	(a)	(a)
9		53.8	7.1	36.7	−5.3	45.5	3.7	35.8	−1.8	(a)	(a)	(a)	(a)
10		44.7	7.0	30.1	−5.5	50.8	4.1	37.2	−1.4	(a)	(a)	(a)	(a)
11		48.5	6.9	31.2	−5.3	52.8	3.9	37.6	−2.2	(a)	(a)	(a)	(a)
12		47.4	7.0	31.2	−5.6	52.3	4.2	37.7	−1.6	(a)	(a)	(a)	(a)
13		46.0	7.1	27.4	−5.3	52.5	4.7	38.0	−2.1	(a)	(a)	(a)	(a)
14		46.1	7.2	29.2	−5.5	53.5	4.2	37.8	−2.3	(a)	(a)	(a)	(a)
15		23.5	9.0	9.3	−5.7	22.5	8.2	9.3	−5.3	20.0	7.0	9.1	−4.8
16		20.4	9.2	8.0	−5.5	20.5	8.6	8.4	−5.0	19.2	7.3	8.8	−4.4
17		8.7	9.1	1.6	−3.5	8.5	8.7	1.6	−3.6	7.5	8.2	1.4	−3.6
18	45	----	----	48.0	−3.3	(a)	(a)	(a)	(a)	(a)	(a)	(a)	(a)
19		59.0	7.3	44.0	−5.8	(b)	(b)	(b)	(b)	(a)	(a)	(a)	(a)
20		60.0	7.4	44.8	−5.4	(b)	(b)	(b)	(b)	(a)	(a)	(a)	(a)
21		20.7	9.2	10.1	−6.5	19.9	7.9	10.7	−5.7	16.6	5.9	10.6	−4.1
22		21.0	9.2	10.1	−6.2	19.8	7.9	10.9	−5.5	----	----	----	----
23		8.0	9.2	2.8	−4.7	8.0	8.8	2.7	−4.7	7.1	8.1	2.3	−4.6
24		8.6	9.4	2.4	−4.5	7.6	8.9	2.4	−4.5	6.8	8.2	2.4	−4.3

[a]Pressure gage not covered with water.

[b]From the shape of the time-history record of the pressure on this gage it appears that the gage is not completely covered with water.

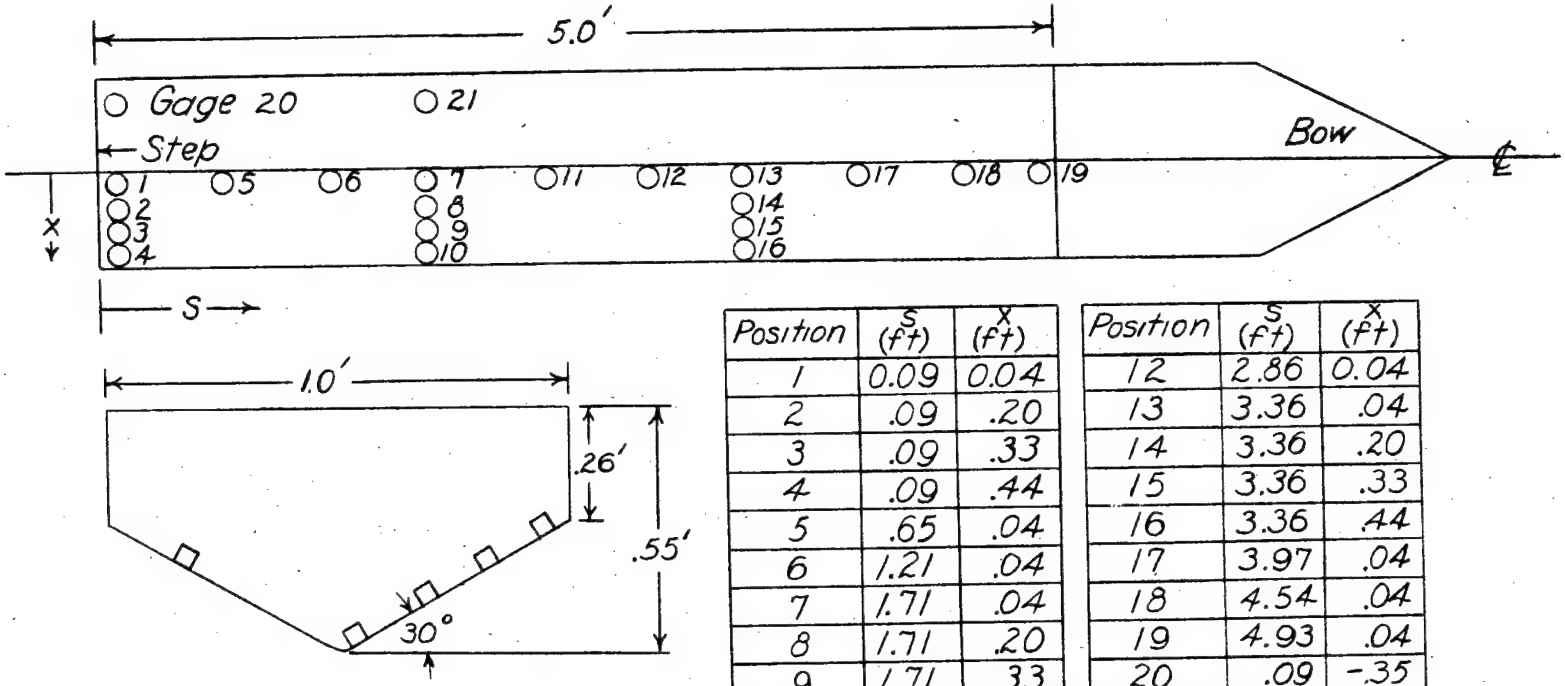

Position	S (ft)	X (ft)
1	0.09	0.04
2	.09	.20
3	.09	.33
4	.09	.44
5	.65	.04
6	1.21	.04
7	1.71	.04
8	1.71	.20
9	1.71	.33
10	1.71	.44
11	2.33	.04

Position	S (ft)	X (ft)
12	2.86	0.04
13	3.36	.04
14	3.36	.20
15	3.36	.33
16	3.36	.44
17	3.97	.04
18	4.54	.04
19	4.93	.04
20	.09	-.35
21	1.71	-.35

NACA

Figure 1.- Hull lines and pressure-gage positions on the model.

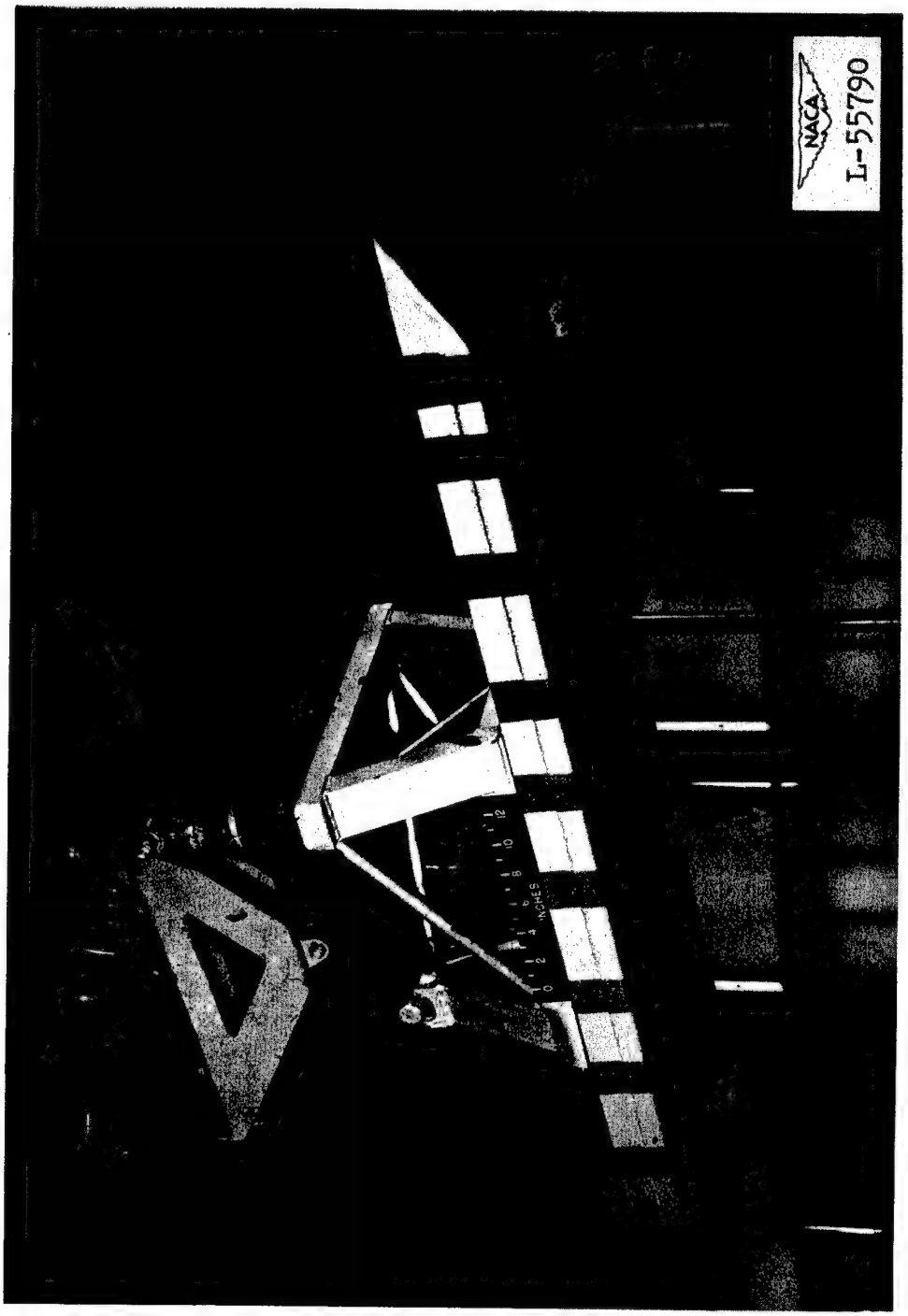

Figure 2.- Model having 30° angle of dead rise.

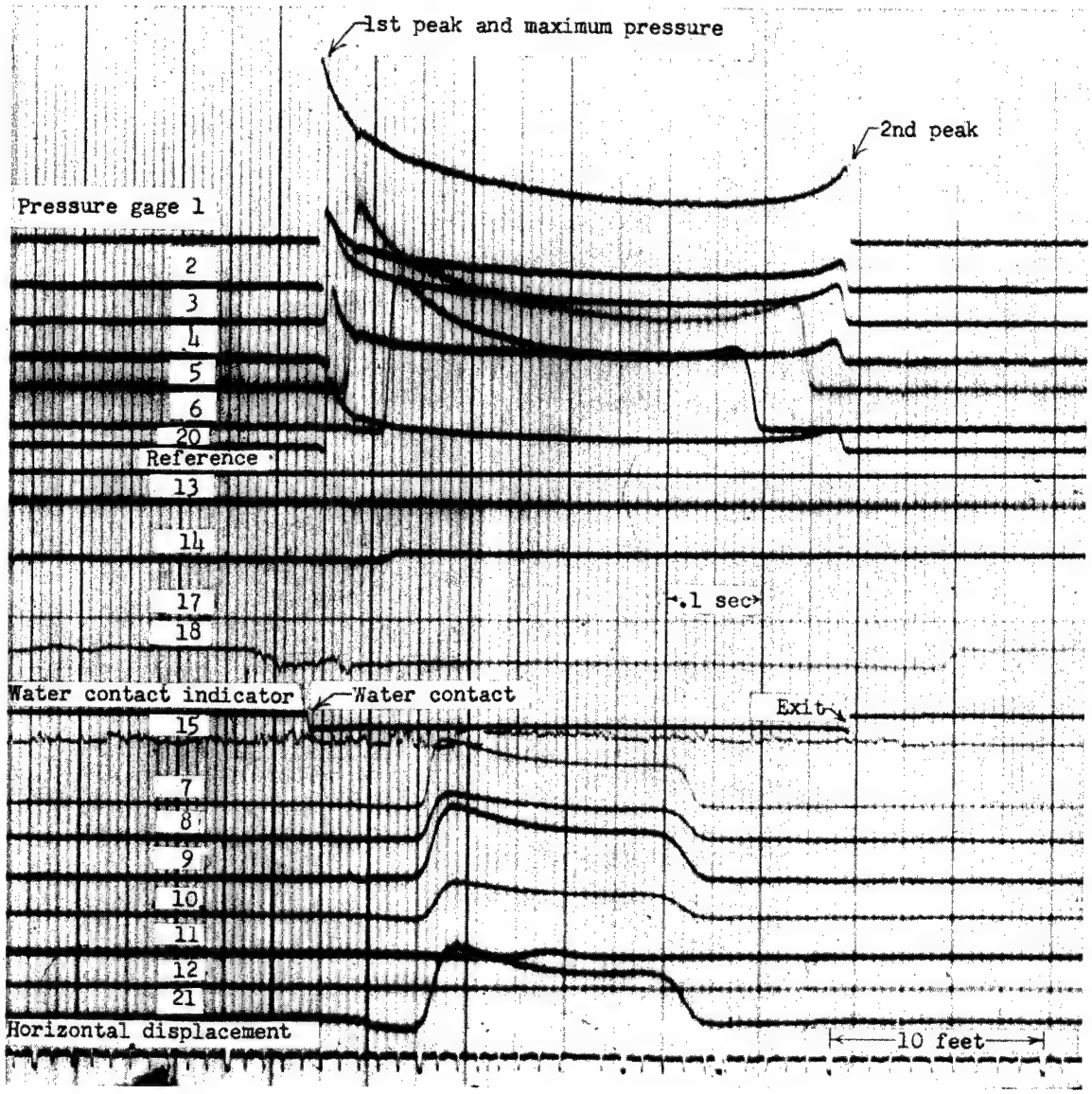

Figure 3.- Typical oscillograph record.

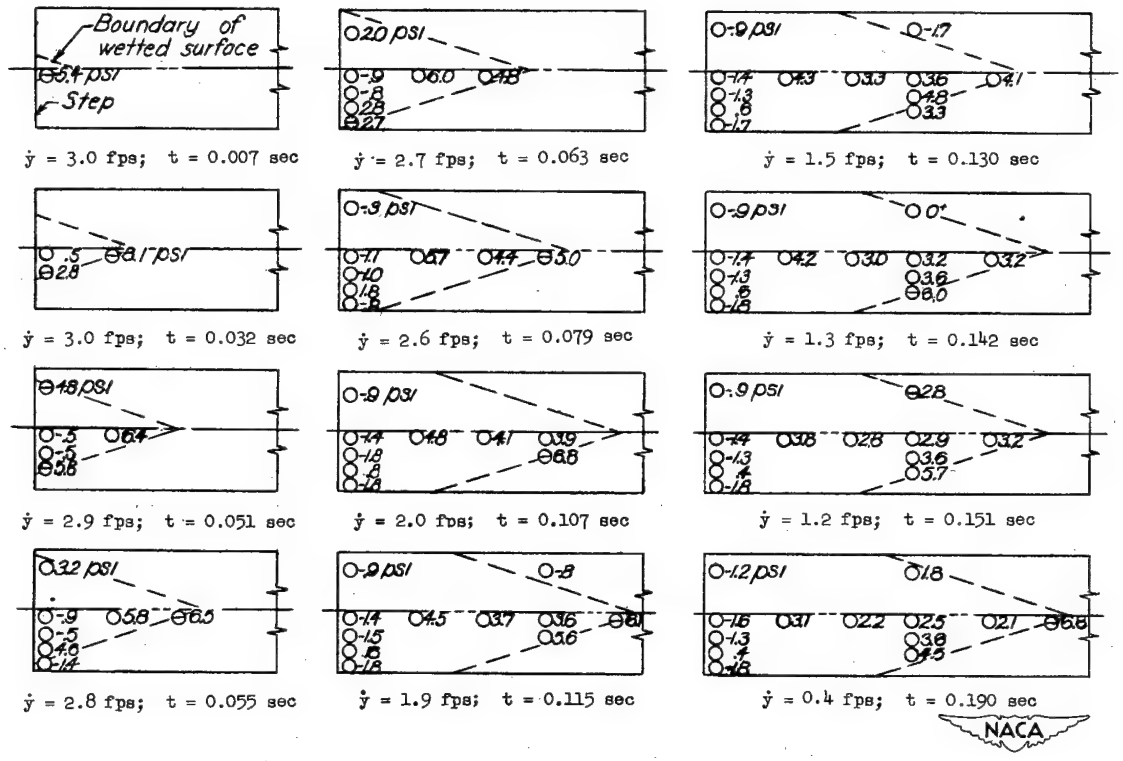

(a) Run 2: $\tau = 6^{\circ}$; $\dot{x}_o = 89.3$ feet per second; $\dot{y}_o = 3.0$ feet per second.

Figure 4.- Instantaneous pressure distributions on the model with 30° angle of dead rise. (Θ indicates the maximum reading of gage during this impact.)

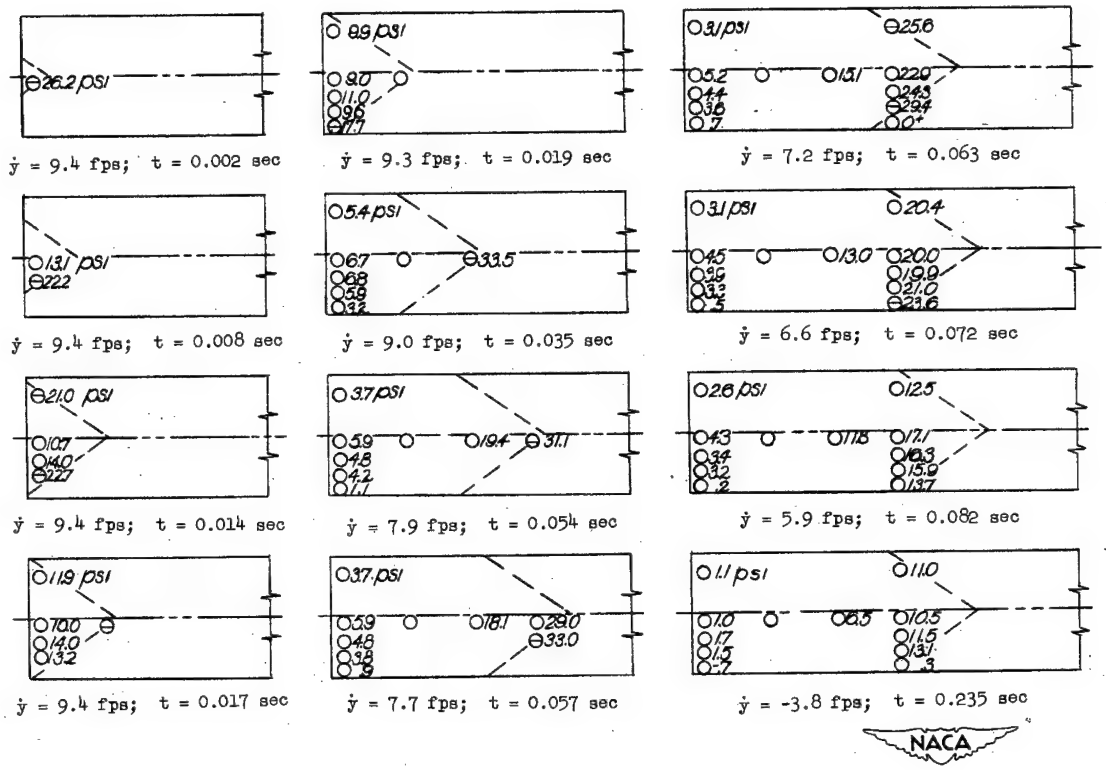

(b) Run 7: $\tau = 15^{\circ}$; $\dot{x}_o = 90.9$ feet per second; $\dot{y}_o = 9.4$ feet per second.

Figure 4.- Continued.

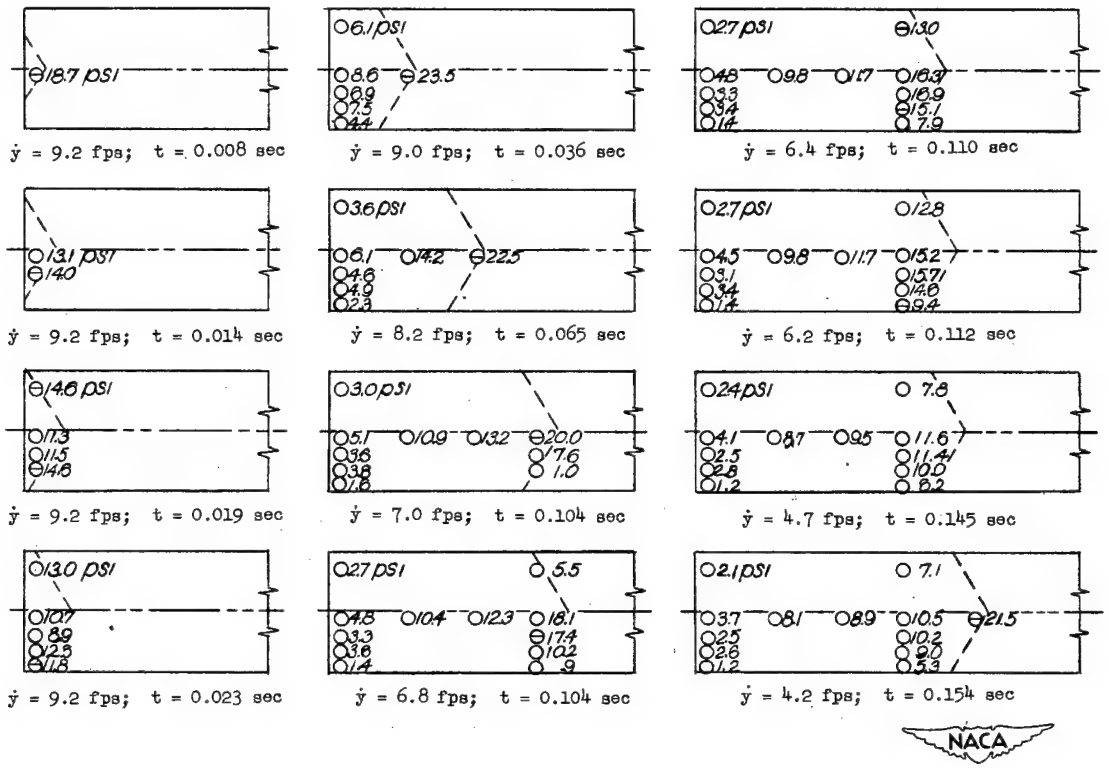

(c) Run 15: $\tau = 30^{\circ}$; $\dot{x}_o = 51.6$ feet per second; $\dot{y}_o = 9.3$ feet per second.

Figure 4.- Continued.

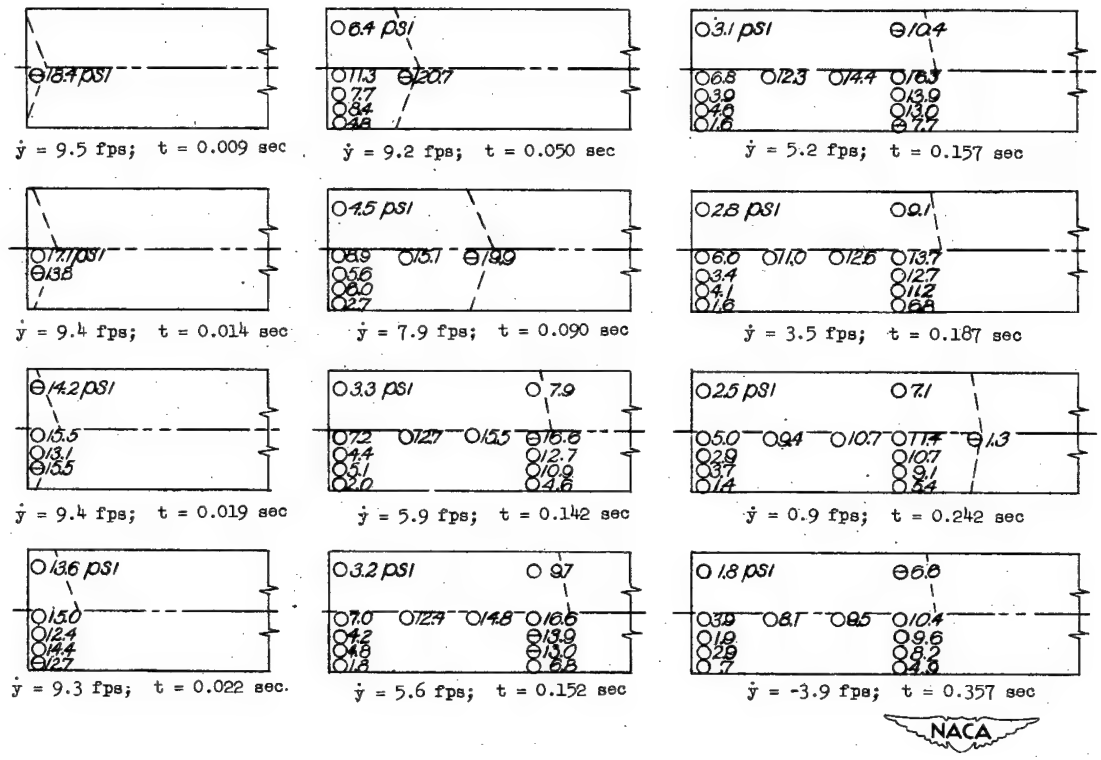

(d) Run 21: $\tau = 45^{\circ}$; $\dot{x}_o = 50.5$ feet per second; $\dot{y}_o = 9.5$ feet per second.

Figure 4.- Continued.

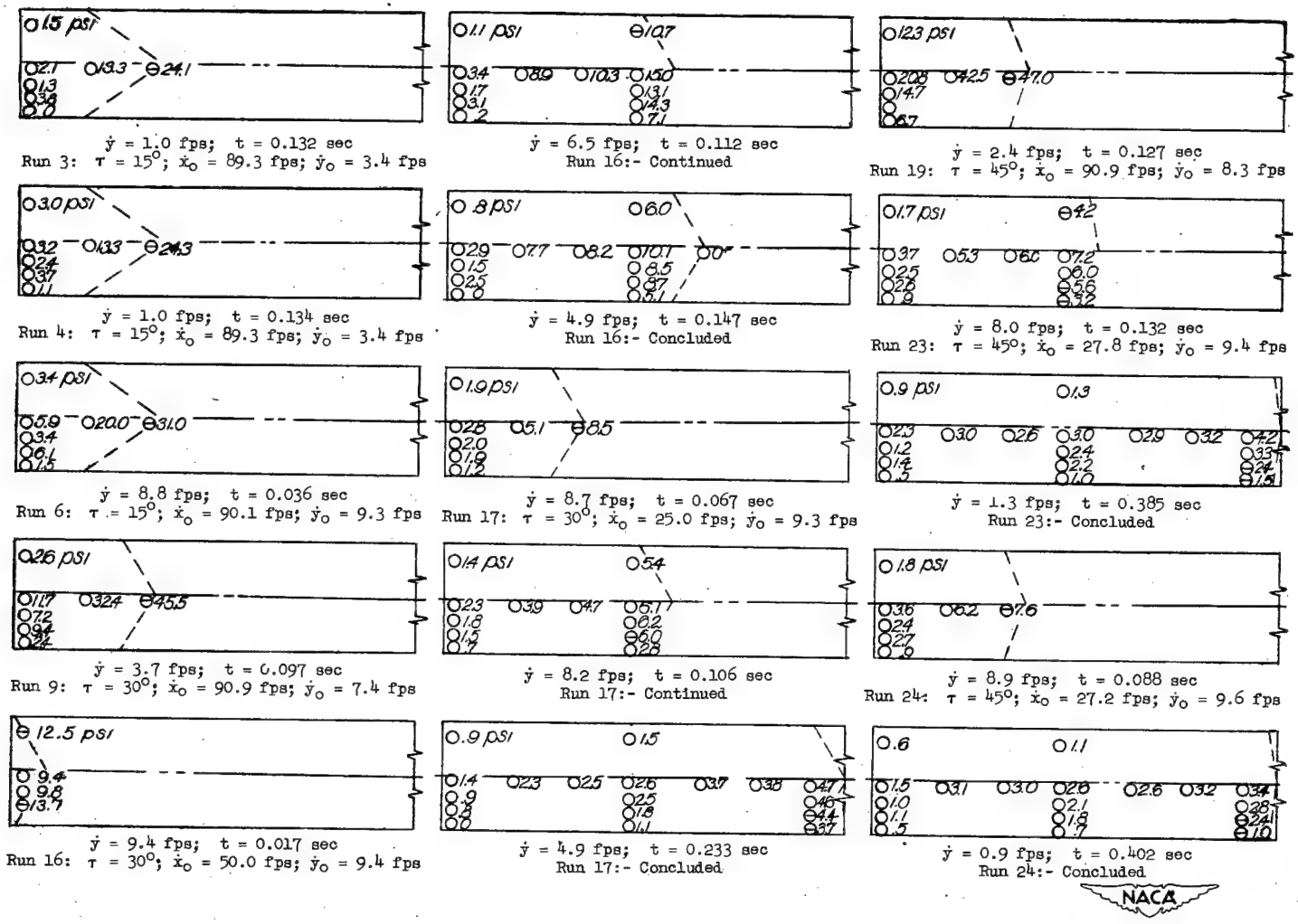

(e) Runs 3, 4, 6, 9, 16, 17, 19, 23, and 24.

Figure 4.- Concluded.

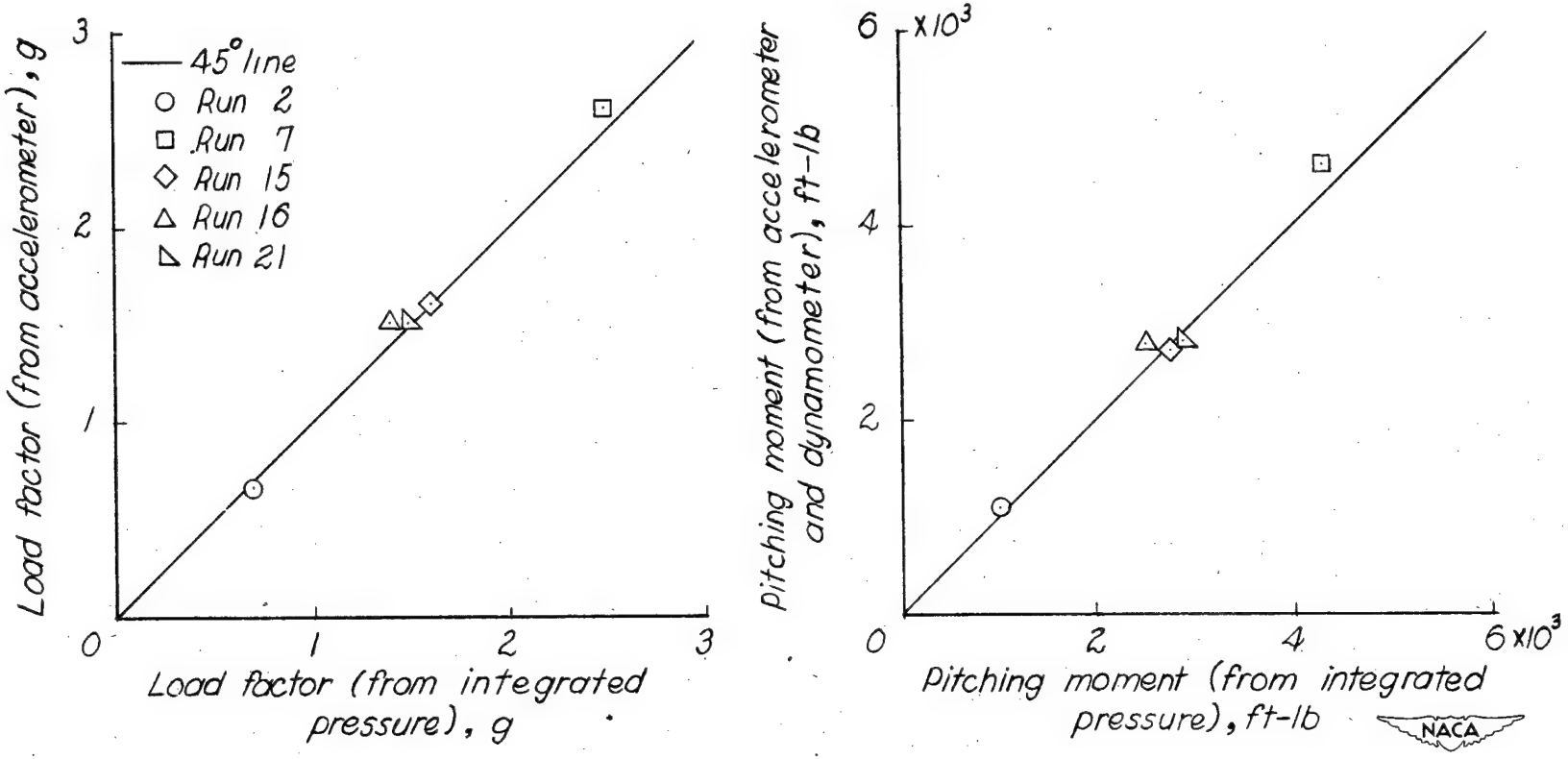

(a) Maximum vertical load factor.

(b) Pitching moment about step at time of maximum load.

Figure 5.- Comparison of experimental measurements of over-all loads and pitching moments with corresponding values obtained by integration of experimental pressure distributions.

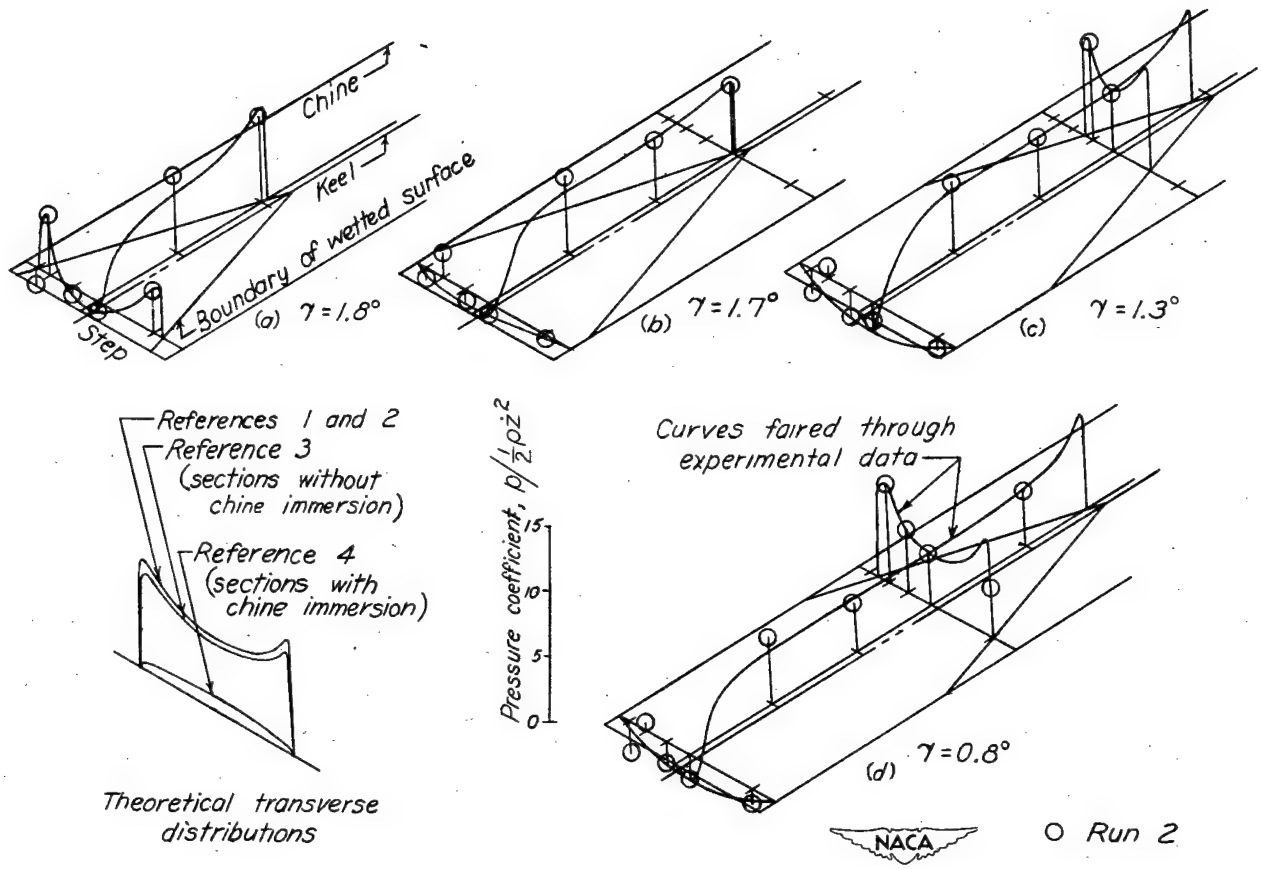

Figure 6.- Variation of instantaneous pressure coefficient $\frac{p}{\frac{1}{2}\rho\dot{z}^2}$ at successive stages of immersion for 6° trim.

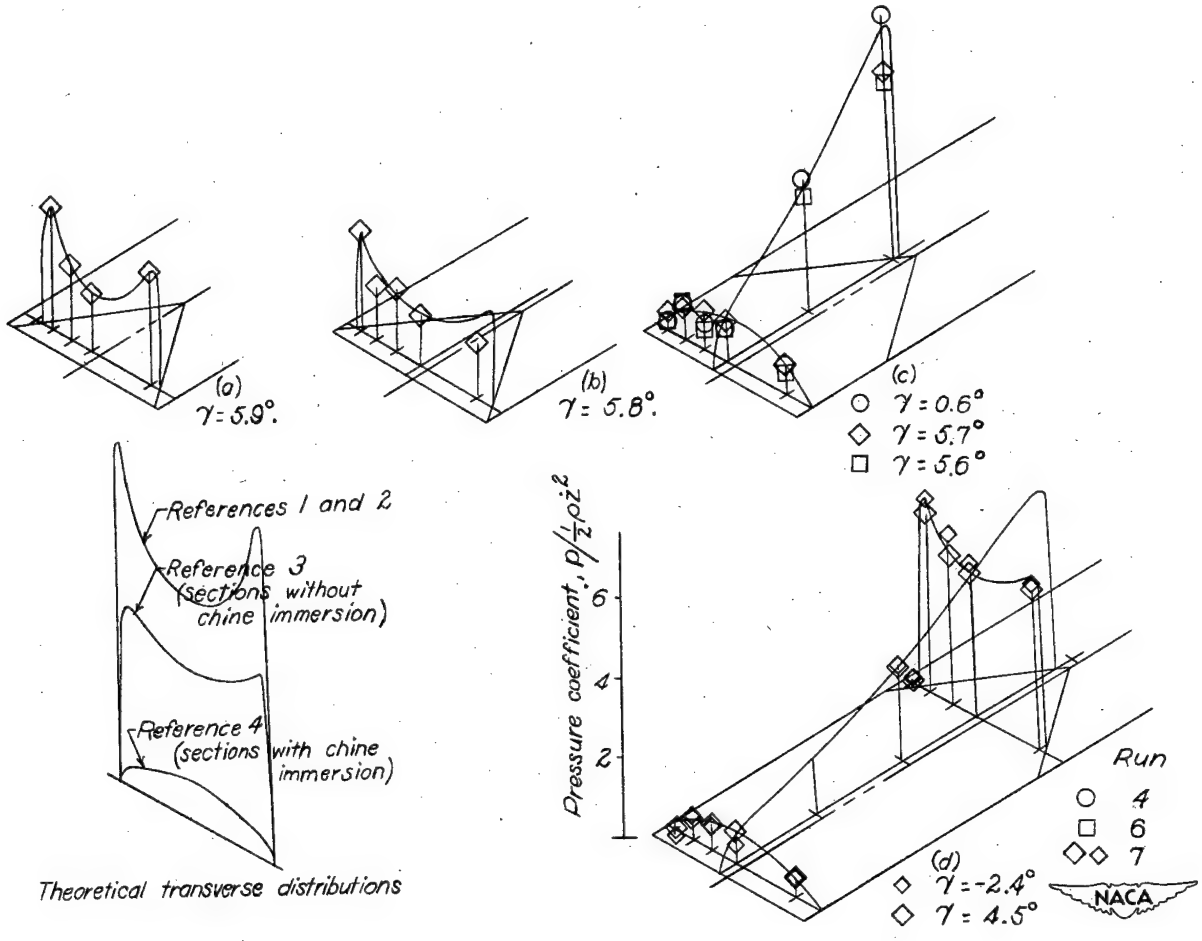

Figure 7.- Variation of instantaneous pressure coefficient $\frac{p}{\frac{1}{2}\rho \dot{z}^2}$ at successive stages of immersion for 15° trim.

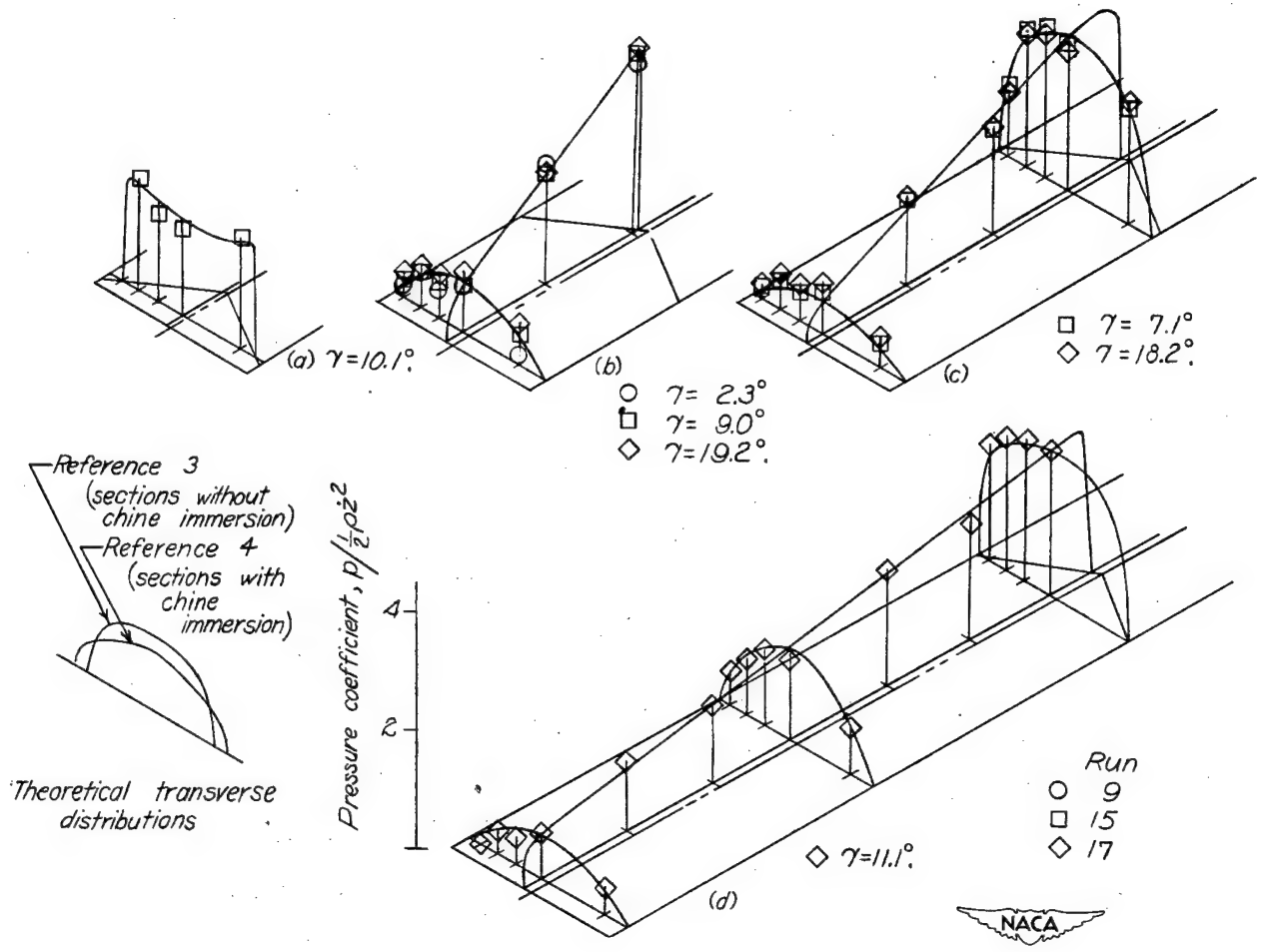

Figure 8.- Variation of instantaneous pressure coefficient $\frac{p}{\frac{1}{2}\rho \dot{z}^2}$ at successive stages of immersion for 30° trim.

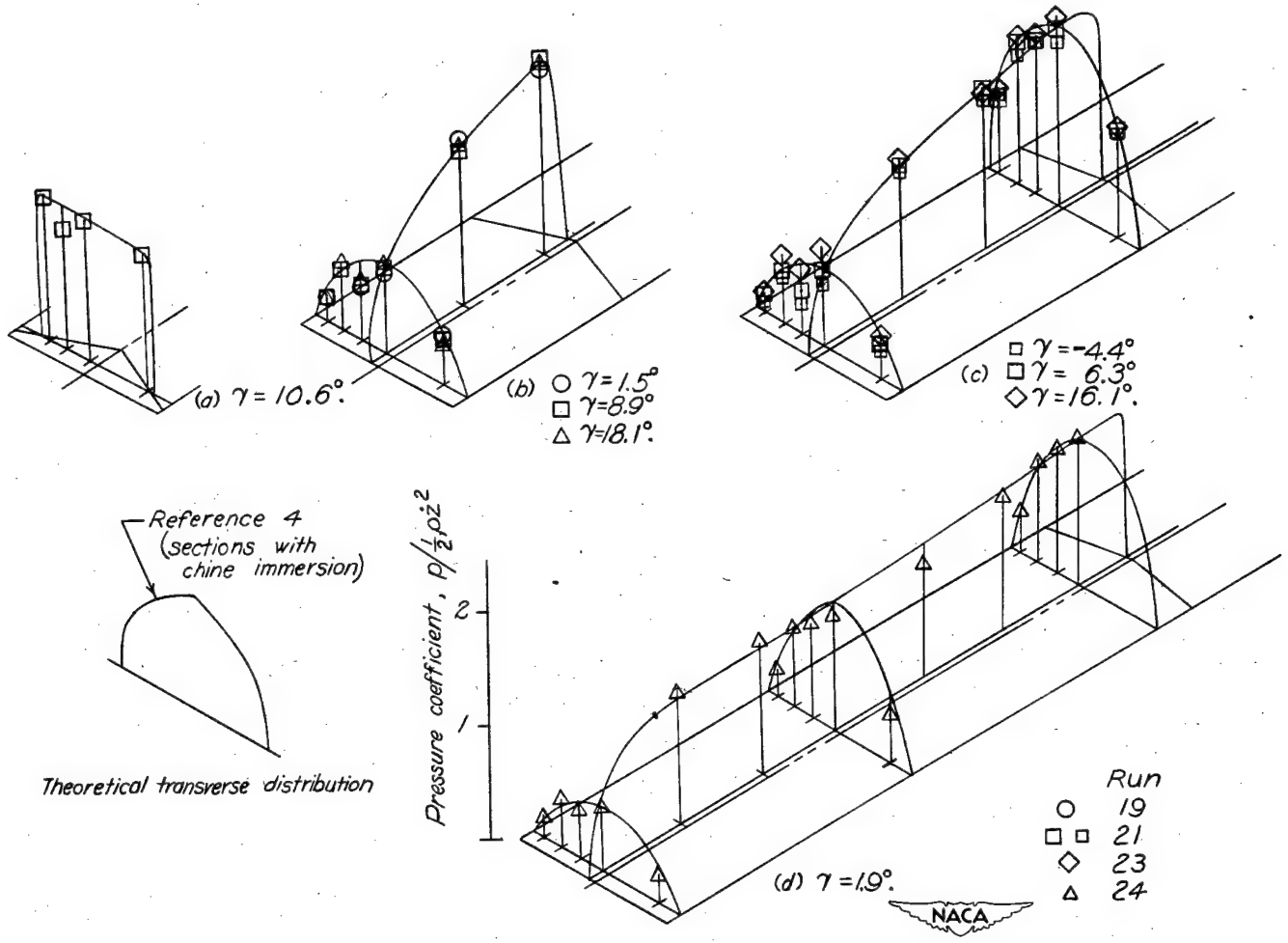

Figure 9.- Variation of instantaneous pressure coefficient $\frac{p}{\frac{1}{2}\rho z^2}$ at successive stages of immersion for 45° trim.

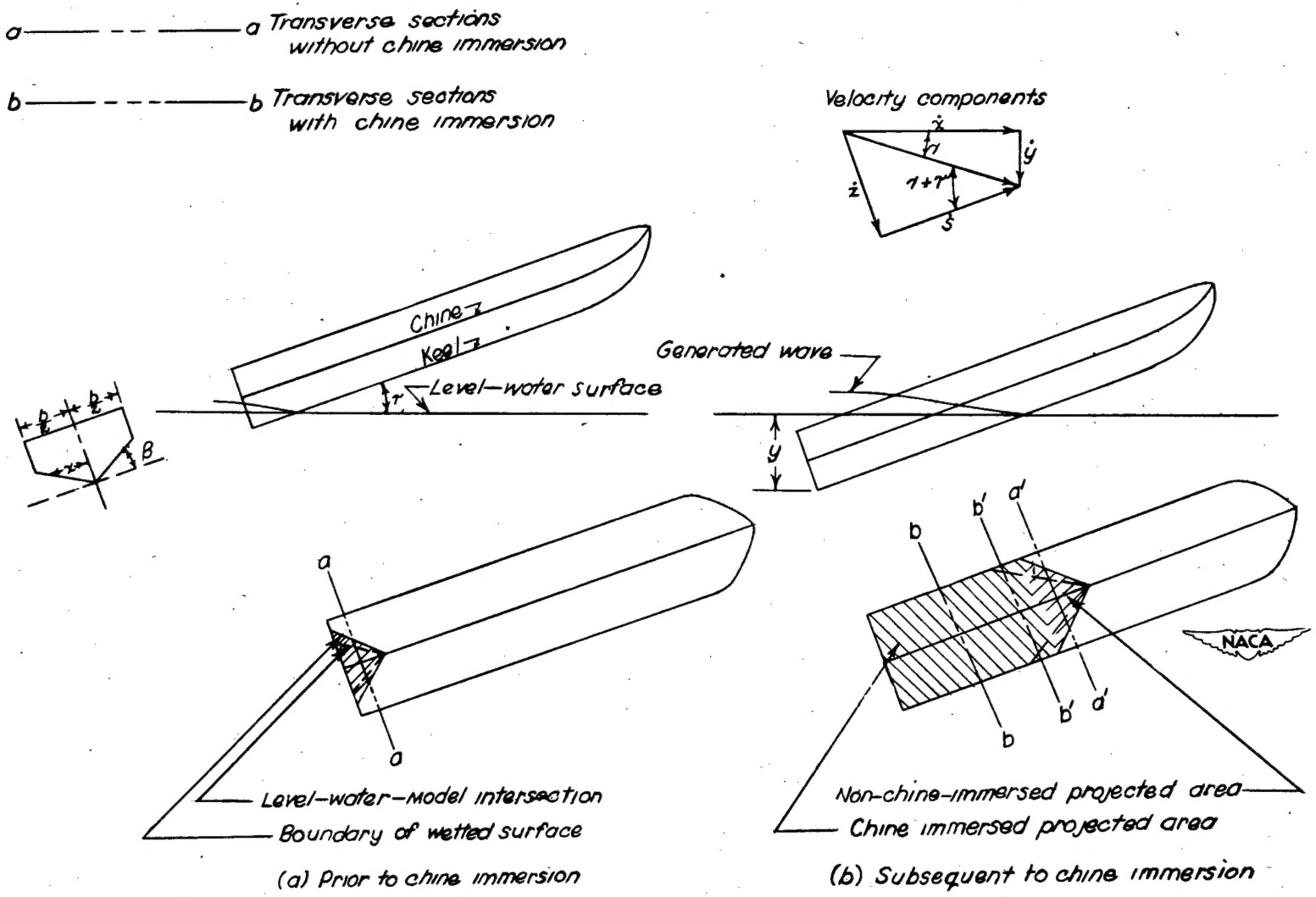

Figure 10.- Schematic diagram of landing.

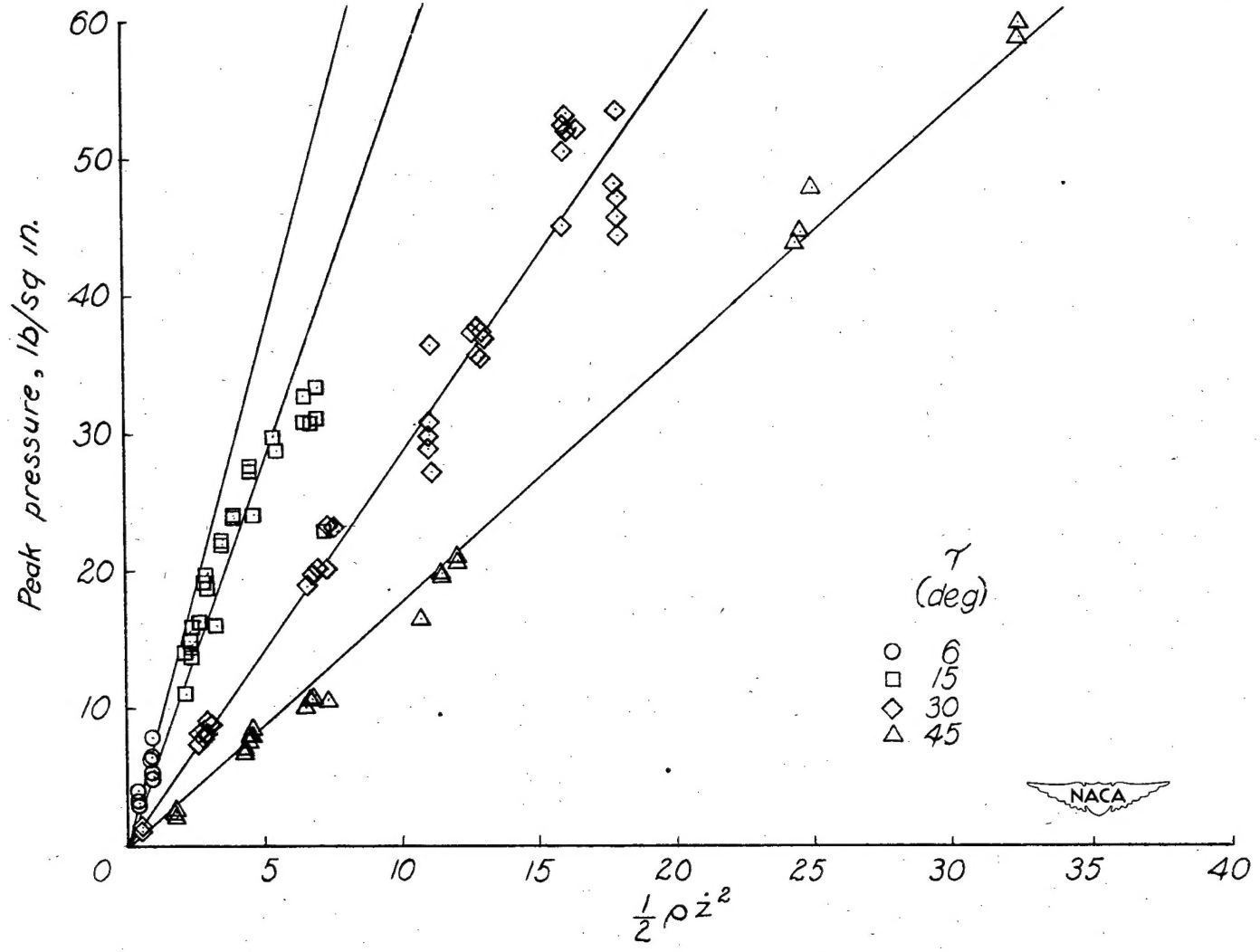

Figure 11.- Variation of peak pressure with $\frac{1}{2}\rho\dot{z}^2$ for various trims.

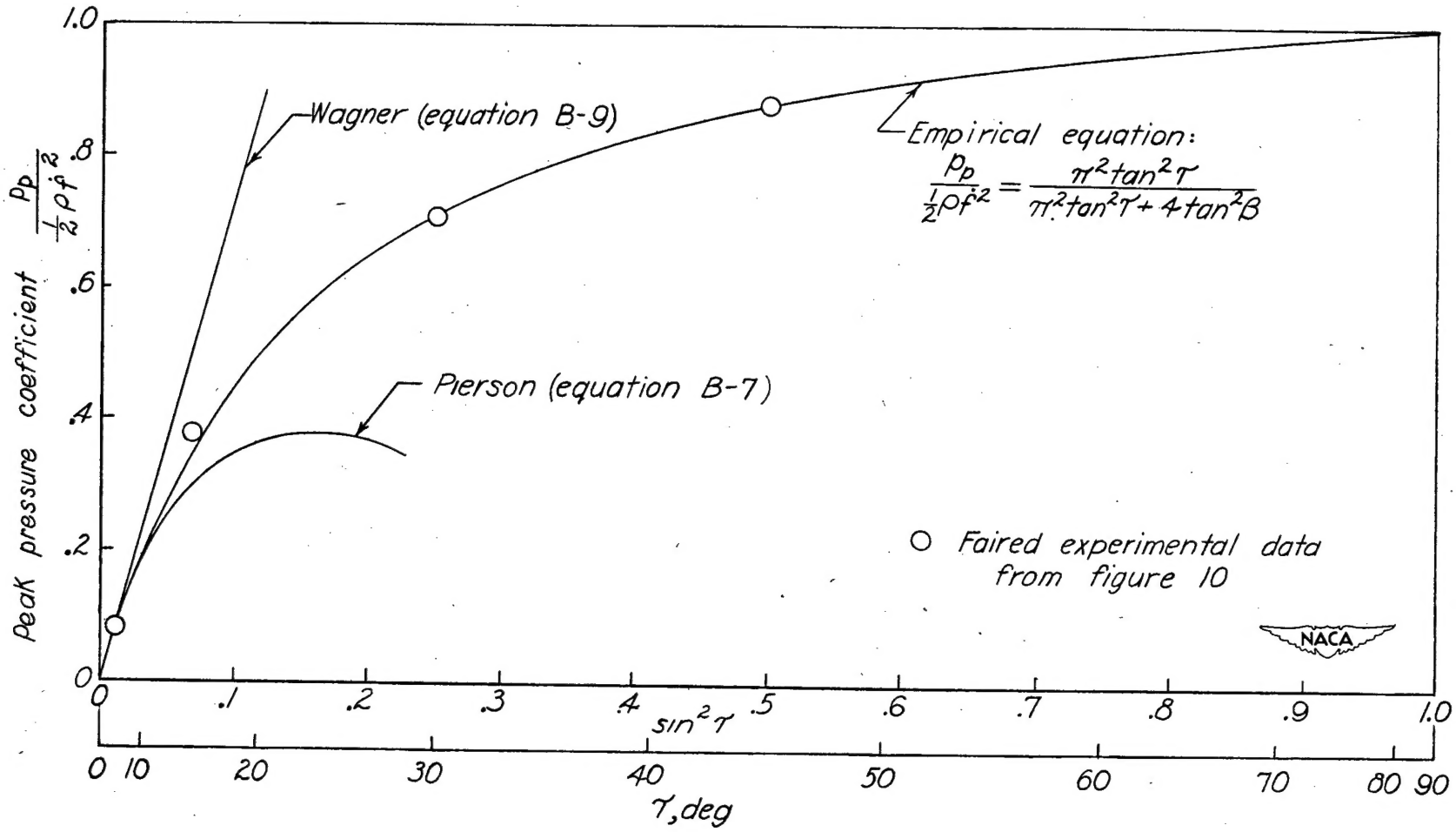

Figure 12.- Variation of peak pressure coefficient $\frac{p_p}{\frac{1}{2}\rho f^2}$ with trim.

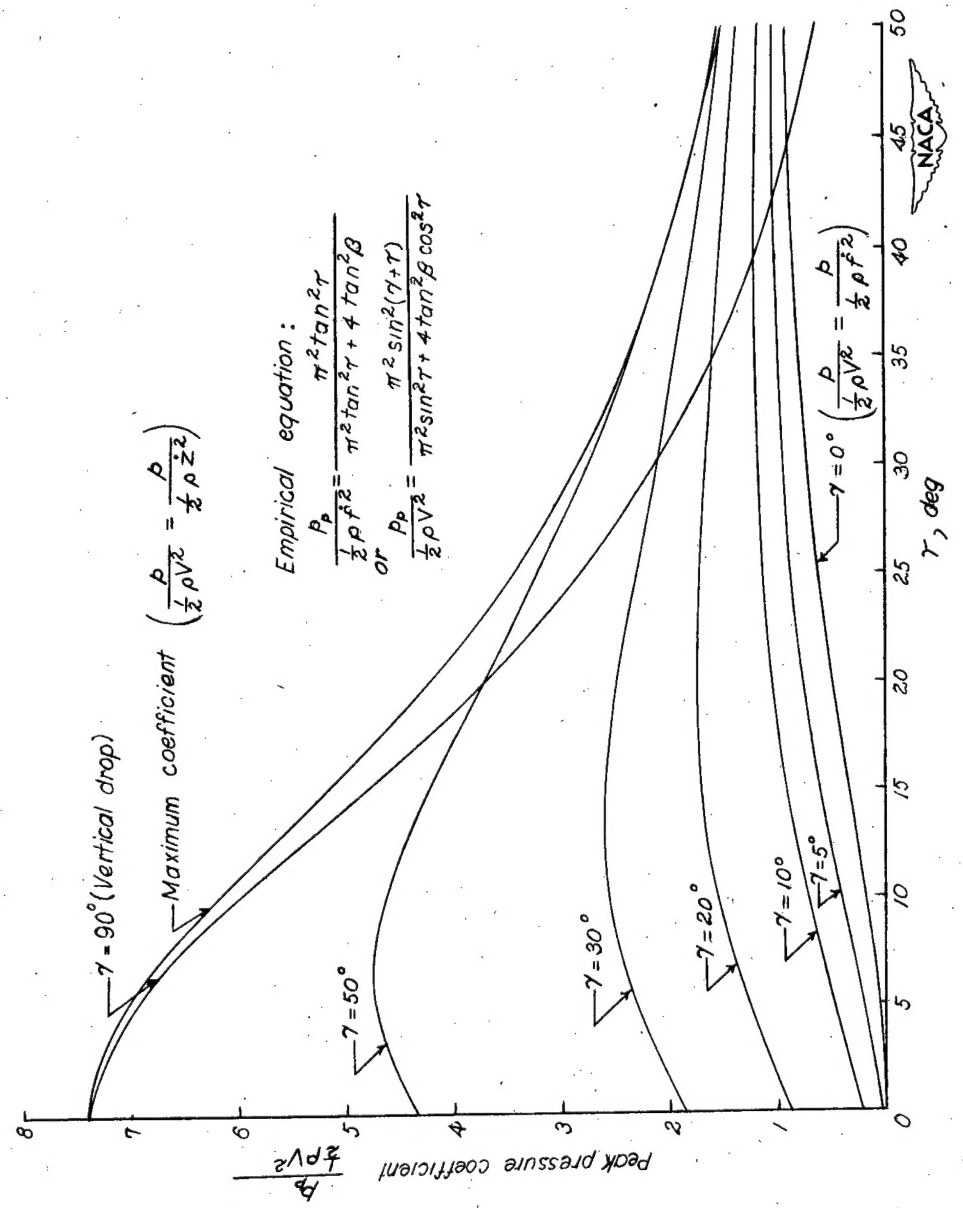

Figure 13.- Variation of peak pressure coefficient $\frac{p_p}{\frac{1}{2}\rho V^2}$ with trim for various flight-path angles.